2017-04-01

Assessment of the energy extraction potential at tidal sites around the Channel Islands

Coles, Danny
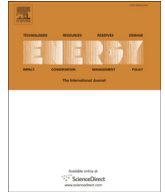
http://hdl.handle.net/10026.1/20338

Assessment of the energy extraction potential at tidal sites around the Channel Islands

D.S. Coles [*], [1], L.S. Blunden [1], A.S. Bahaj [1]

Energy and Climate Change Division, Sustainable Energy Research Group, Faculty of Engineering and the Environment, University of Southampton, UK

ABSTRACT

Tidal flows around the Channel Islands contain a significant energy resource that if harnessed could provide electrical power to the Channel Islands, the UK and France. We have developed a new 2D hydrodynamic model of the English Channel which gives an improvement to the temporal and spatial resolution of the ambient flow in comparison with previous regional scale resource assessments. The ambient flow was characterised to identify suitable sites, resulting in a reduction in total development area of up to 80% compared with previous studies. Estimates for upper bound energy extraction confirm that Alderney Race contains the majority of the Channel Islands resource, giving a maximum potential of 5.1 GW, which exceeds a previous estimate for the Pentland Firth by 35%. This is followed by Casquets (0.47 GW) and then Big Roussel (0.24 GW). Our work shows that energy extraction at Alderney Race has a constructive impact on the resource at Casquets, and that the sensitivity to added drag at each site with respect to energy extraction is highly dependent on bathymetry and the proximity of coastlines. These results have implications for the overall resource development within the Channel Islands, where regulation is needed to account for site-site interaction.

1. Introduction

The Channel Islands are a collection of five main islands located to the west of the Cotenin Peninsula in Normandy, France (Fig. 1). In reports commissioned by the Carbon Trust [1,2] five sites were identified as suitable for tidal energy development based on tidal current velocities (mean neap peak and mean spring peak velocities), bathymetry and available area. These include three main sites of medium to high potential (Alderney Race, Casquets and Big Roussel) and two low potential sites off the North West coast of Guernsey and off the North East coast of Jersey.

Estimates for energy extraction at these sites vary significantly depending on the method used and the scheme areas and array design considered. This is demonstrated in Table 1, which summarises the range of results from previous assessments of Alderney Race, Casquets and Big Roussel. In general, past studies have relied on low spatial and temporal resolution flow data, which

may have impacted on the derived results. Additionally methods such as the farm and kinetic flux approaches adopted in the past [3,4,2] assume no change to the ambient flow field with the inclusion of turbines (i.e. no consideration into blockage effects), bringing into question the validity of these results. Other studies assume a 5% wake deficit within turbine arrays [5], yet they still do not consider the array scale blockage caused by the considerable added drag by large arrays. For further information on the farm and kinetic flux methods we recommend the reader consults the references given in Table 1.

We recognise that previous studies have provided a knowledge enhancement for assessing the tidal energy resource at sites within the Channel Islands. However, the varied approach to site characterisation, energy extraction model and scarcity of reliable flow data makes it difficult to make direct comparisons of the resource at each location. To address this problem a well-established method for quantifying an upper bound for power extraction (termed the maximum average power potential) was implemented here for sites in the Channel Islands using a new 2D hydrodynamic model of the English Channel. The method is described below and in more detail in §2.4, and is the same approach as has been conducted in literature to estimate the maximum average power potential of the

* Corresponding author.
  E-mail address: d.coles@soton.ac.uk (D.S. Coles).
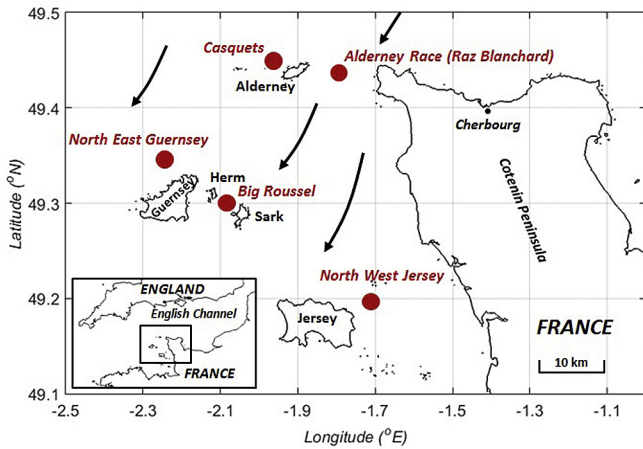[1] www.energy.soton.ac.uk.

Fig. 1. Location of potential sites for tidal energy development in the Channel Islands [1], located off the west coast of Normandy, France. Arrows show the direction of dominant ebb tide. The relative location of the Channel Islands to the UK and France is shown inset.

Pentland Firth in Scotland [6] and Minas Passage [7,8], Johnstone Strait [9] and Masset Sound [10] in Canada.

Within the hydrodynamic model, a drag is distributed uniformly over 'energy extraction zones' that span the entire width of a site. This is done to simulate momentum extraction by large tidal stream turbine arrays. The total power extracted from the flow by the added drag within the energy extraction zone is calculated and averaged over time to give an 'average power potential'. This is not to be confused with the *available* power, which is the fraction of the extracted power that is removed by the turbines (which is used directly for electricity generation) [6]. To simulate the effect of adding more turbines, the drag distributed over the energy extraction zone is increased, resulting in an increase in the hydrostatic pressure force driving the flow through the zone, seen as an increase in the difference between free surface elevation upstream and downstream of the energy extraction zone. This added drag reduces the volume flux through the energy extraction zone. Assuming alternative flow paths exist, the increase in hydraulic resistance caused by the added drag also causes flow to divert around the energy extraction zone, taking the path of least resistance. The extracted power within the energy extraction zone is the product of the head loss across the energy extraction zone and the volume flux through the energy extraction zone. Initially, as drag is

added there is an increase in the head drop across the energy extraction zone, which has a dominating effect over the decrease in volume flux, causing the extracted power to increase. As the uniformly distributed drag is increased further, the reduction in volume flux has an increasingly significant effect over the increase in head drop, where at the upper bound it suppresses the increase in head drop, initiating a decrease in the extracted power. The maximum average power potential is the upper bound limit of the average power potential. It is the maximum power that can be extracted by adding a uniform drag over the energy extraction zone, where any further increase in drag causes a reduction in the extracted power.

The information in the paper is organised as follows: in §2 a new 2D hydrodynamic model of the English Channel is presented, which simulates flow around the Channel Islands at significantly improved spatial and temporal resolution compared with previous regional scale studies summarised in Table 1. Model validation results are presented in §3 using elevation data at 13 ports around the domain, as well as flow data obtained from Acoustic Wave and Current Profiler (AWAC) deployments in Alderney Race. Such combination of validation datasets gives confidence in the model's ability to accurately recreate tidal flows around the Channel Islands. Ambient flow distribution results are presented in §4.1, which were used to quantify the distribution in mean kinetic power density at Alderney Race, Casquets, Big Roussel, North West Guernsey and North East Jersey. In §4.2 estimates for the power potential at suitable sites are given, and comparisons are made with estimates for the maximum average power potential at the Pentland Firth in Scotland [6], Minas Passage [7,8], Johnstone Strait [9] and Masset Sound [10] in Canada (Table 6). In §4.3 the level of interaction between each site is investigated by simulating simultaneous energy extraction scenarios. This is novel as it is the first time site-site interaction has been quantified for sites around the Channel Islands. In §4.4 results are presented that consider more realistic levels of array drag based on the physical constraints of turbine spacing. Power extraction from these more realistic simulations are compared with the upper bound solutions from §4.2 and §4.3 to comment on the possible level of tidal energy development at each site. In §4.5 the available power is estimated by implementing the realistic level of drag at each site. The available power is defined as the fraction of the extracted power that is removed by ideal tidal turbines for electrical power production [6]. In §4.6 the effect of added drag on the surrounding flow field is plotted and the change in volume flux through each site is quantified.

Table 1
Results from literature showing methods used, array capacity and electricity generation from Alderney Race, Casquets and Big Roussel.

| Method	Studies	Array scheme area or cross section	Array capacity (GW)	Annual electricity generation (TWh/year)
Alderney Race				
Farm	ETSU [3], European Commission [4], Bahaj et al. [10], Myers et al. [11]	65 km^2–102 km^2	0.84–2.4	1.35–7.4
Kinetic energy flux	Black and Veatch, Phase I [2], Black and Veatch, Phase II [2], Owen [11]	3.3 km–5.5 km wide cross sections	NA	0.37–1.37
Power potential	Black and Veatch, Phase III [12]	5 km wide cross section	NA	2.25
Casquets				
Farm	ETSU [3], European Commission [4]	190 km^2–215 km^2	0.37–2.5	1.3–2.9
Kinetic energy flux	Black and Veatch, Phase I [2], Black and Veatch, Phase II [2], Owen [11]	8 km wide cross section	NA	0.4–1.6
Power potential	Black and Veatch, Phase III [12]	61 km^2	NA	1.9
Big Roussel				
Farm	ETSU [3]	90 km^2	2.5	2
Kinetic energy flux	Black and Veatch, Phase I [2], Owen [11]	2.7–4 km wide cross section	NA	0.16–0.3
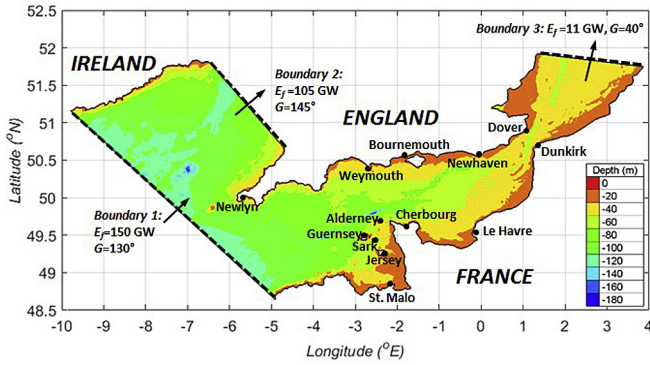
Fig. 2. English Channel Model domain in Universal Transverse Mercator (UTM) projection, showing the location of three open boundaries and depth in metres. The location of thirteen ports used for validation in §3.1 are also shown. G is the phase of the M_2 tide and E_f is the time averaged energy flux through each open boundary.

2. English Channel model

2.1. Domain

Telemac 2D [13] was used to build a new 2D hydrodynamic model of the English Channel. The domain covers the whole of the English Channel with open boundaries in the Atlantic Ocean, Irish Sea and the North Sea (Fig. 2). The location of the three boundaries overlay validated elevation gauge measurements from the TPXO European Shelf 2008 solution [14]. Reducing the size of the domain gave unsatisfactory validation results and was therefore not pursued further. The closest boundary to the Channel Islands is the

Atlantic Ocean boundary (approximately 350 km away). A preliminary study was conducted to investigate the far field effects of power extraction at Alderney Race, Casquets and Big Roussel on the open boundaries. It was found that this did create back effects on the open boundaries, however changes in velocity at the boundaries were limited to below 0.01% which was deemed acceptable. Fig. 2 also shows the average energy flux E_f through each of the three open boundaries due to the M_2 tide, which was calculated using Equation (1) [15], where ρ is water density, g is acceleration due to gravity, h is water depth, u is the depth averaged velocity perpendicular to the boundary, ζ is free surface elevation and Γ denotes the line drawn by each open boundary, segmented by length s. The overbar denotes time average over the period of the M_2 tidal cycle.

$$E_f = \rho g \int_{\Gamma} h\overline{u\zeta}ds \qquad (1)$$

The arrows and phase G of the M_2 tide through each boundary (shown in Fig. 2) indicate the phase lag between the M_2 wave entering the domain in the Celtic Sea (Boundary 1) and leaving the domain through the Irish Sea (Boundary 2) and the North Sea (Boundary 3).

2.2. Governing equations

The model solves the shallow water equations using the finite element method. The shallow water equations are applicable for cases where the horizontal length scale is greater than the vertical length scale, such that the vertical velocities are negligible and the pressure can be treated as hydrostatic. Under this assumption, and
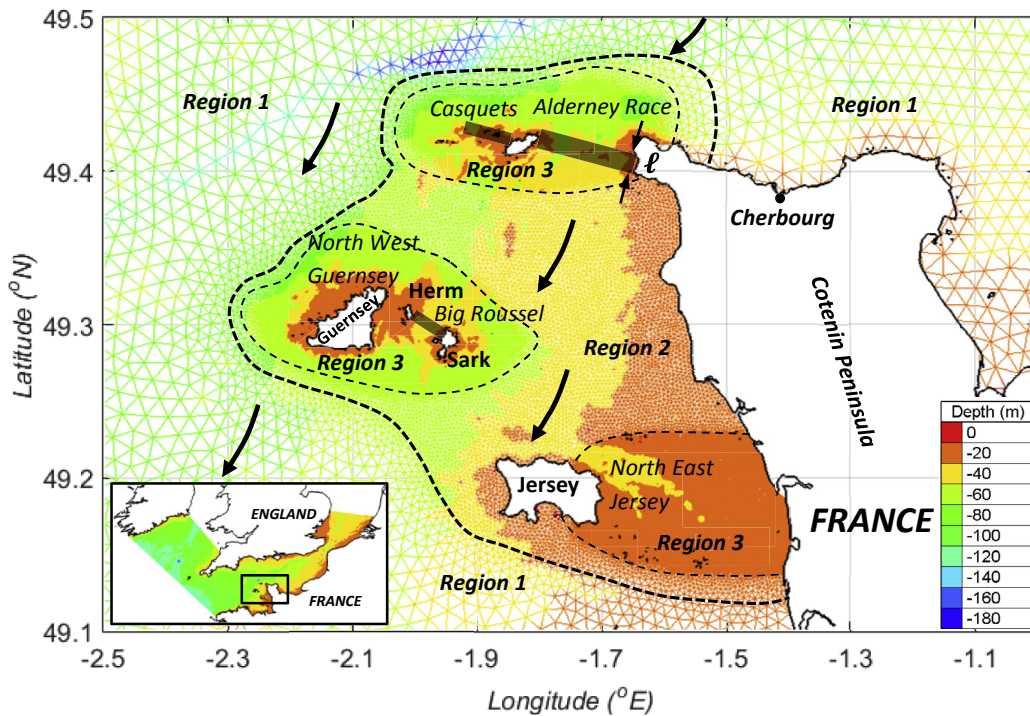
Fig. 3. Mesh resolution in and around the Channel Islands, showing 250 m mesh resolution around Alderney Race, Casquets, Guernsey, Herm and Sark and North East Jersey (Regions 3), 1 km mesh resolution around the Channel Islands (Region 2) and 5 km mesh resolution elsewhere (Region 1). The 3 shaded (grey) regions at Alderney Race, Casquets and Big Roussel show the location of the energy extraction zones where added drag is applied. ℓ is the fetch of the energy extraction zone spanning shown for the Alderney Race only. Arrows show the direction of the dominant ebb tide. The model domain is inset.

neglecting other forcing such as wind and buoyancy, depth integration of the Navier-Stokes equations for an incompressible fluid reduces to the shallow water equations solved simultaneously by Telemac 2D [16]:

$$\text{Continuity}: \quad \frac{\partial h}{\partial t} + u \cdot \overrightarrow{\nabla}(h) + h\nabla \cdot (\overrightarrow{u}) = S_h \tag{2}$$

$$\text{Momentum along } x: \quad \frac{\partial(u)}{\partial t} + \overrightarrow{u} \cdot \overrightarrow{\nabla}(u)$$
$$= -g\frac{\partial Z}{\partial x} + S_x + \frac{1}{h}\nabla(h\nu_t \overrightarrow{\nabla}u) \tag{3}$$

$$\text{Momentum along } y: \quad \frac{\partial(v)}{\partial t} + \overrightarrow{u} \cdot \overrightarrow{\nabla}(v)$$
$$= -g\frac{\partial Z}{\partial y} + S_y + \frac{1}{h}\nabla \cdot (h\nu_t \overrightarrow{\nabla}v) \tag{4}$$

where u and v are the horizontal depth averaged velocity components aligned with the x and y axis, Z is the free surface elevation, h is depth, ν_t is the momentum diffusion and $S_h/S_x/S_y$ are fluid source/sink terms that include Coriolis acceleration, bottom friction and/or a momentum sink applied in the energy extraction zones. Equations (2)–(4) are a function of spatial position, x and y as well as time, t as a result of direct tidal forcing boundary conditions.

2.3. Pre-processing

Over the majority of the domain TCarta 90 m resolution bathymetry data was used. In regions where the TCarta bathymetry did not cover the domain in the deeper Celtic Sea in close proximity to Boundary 1 (see Fig. 2), bathymetry was obtained from the General Bathymetric Chart of the Oceans (GEBCO) [17] at approximately 900 m resolution. The bathymetry was mapped onto an unstructured mesh (Fig. 3), where mesh independence studies were conducted to ensure free surface elevations at 13 ports around the domain (Fig. 2) were independent of mesh resolution.

Three regions were allocated within the domain based on their likely mesh resolution requirement to capture the necessary scales of flow. Region 1 covers the open sea stretching throughout the majority of the domain where depth is high relative to local changes in bathymetry so that flow gradients are relatively low. In this region free surface elevation amplitudes and phases within the Channel Islands were relatively insensitive to mesh resolution so was kept low at 5 km to improve computational efficiency.

Region 2 incorporates the perimeter of the Channel Islands which roughly follows the 50 m depth contour shown in Fig. 3, the maximum approximate depth for turbines to be installed. Any further decrease in element size below 1 km gave no change in tidal elevation amplitudes and phases so 1 km elements were adopted for this study.

Region 3 covers the five areas of interest for power extraction within the Channel Islands. The mesh within this region was resolved to 250 m mesh resolution, with any further mesh refinement showing no change in free surface elevations or power extraction.

Bed friction was used as a tuning parameter to give improved agreement with free surface elevations and velocity data from Acoustic Wave and Current Profiler (AWAC) deployments within Alderney (see §3 Model validation). A realistic range of bed drag coefficient values were estimated based on measurements of hydraulically rough river flow over gravel beds, where Bray [18] gives an expression for the Nikuradse grain roughness height k_s in terms of the diameter of the roughness d_{90}, with 90% finer by weight:

$$k_s \approx 3d_{90} \tag{5}$$

The bed drag coefficient C_b is approximated as [19]:

$$C_b = 2\left(\frac{\kappa}{\log\left(\frac{12h}{k_s}\right)}\right)^2 \tag{6}$$

where κ is Von Karman constant and h is depth. Alternatively for a flat bed of sediment, k_s is related to the median grain diameter (d_{50}) as approximately $k_s = 2.5d_{50}$ [20], whilst Liu [21] suggests $k_s = mH_r$ for beds with sand ripples where H_r is the ripple height and m varies from 0.5 to 1.0. Based on Equation (6) tuning of C_b was restricted to values less than 0.052, which corresponds to a roughness diameter d_{90} which is 2% of the flow depth h.

To characterise the ambient flow, the dominant $M_2, S_2, N_2, K_2, K_1, O_1, P_1, P_1, Q_1$ and M_4 amplitudes and phases were extracted from the Atlantic Ocean Atlas [22] to drive elevations along the three open boundaries shown in Fig. 2. Non-reflective boundary conditions were applied along the liquid boundaries to allow waves to leave the domain with little or no reflection [13].

The model detects shallow areas where the sea bed becomes exposed due to the high tidal range. The model then corrects free surface gradients in these regions to prevent spurious driving forces occurring on semi-wet elements. A constant turbulent viscosity of 10^{-4} N/m^2 was used as implementing turbulence models did not lead to significant improvement in validation results but did add significantly to computation time. A time step of 1 min was implemented. A total of 152643 elements and 77301 nodes were used in the domain. The accuracy of the propagation step was set to 0.001, which was deemed acceptable without incurring excessive computational cost. The steering file used to run the simulations is included as Appendix A. The geometry file and subroutines and are available from the University of Southampton Sustainable Energy Research Group (SERG) website [23].

2.4. Simulating power extraction

Turbines were simulated by applying an equivalent added drag coefficient C_e to the existing parameterisation of bed friction, applied uniformly over the area of the energy extraction zone, A_z. C_e is parameterised using Equations (7) and (8) [5], where array density λ is defined as the total swept area of n turbines within the energy extraction zone area A_z. A_s is the swept area of an individual rotor and C_D is the turbine drag coefficient which is assumed to remain constant at $C_D = 0.8$ based on turbine thrust measurements from scaled down laboratory testing [24]. This method has recently been validated experimentally for arrays of porous fences [25], where experimental load cell measurements of the total fence drag agreed within 10% of the numerical formulation of array drag given by Equations (7)–(9).

$$\lambda = nA_s/A_z \tag{7}$$

$$C_e = \frac{1}{2}\lambda C_D \tag{8}$$

C_e is added to the bed drag coefficient C_b to give the 2D formulation of combined drag as a shear force, where u is the depth-averaged velocity:

$$\frac{\tau}{\rho} = (C_e + C_b)u^2 \tag{9}$$

The method used here takes the same approach as previous assessments of the Pentland Firth [6] and Vancouver Island [9], so

as to make a direct comparison of the estimated power potential with these sites (see Table 6). To adopt the same approach as these studies, energy extraction zones spanned the entire width of each site to prevent flow diversion around the arrays within the site itself and only M_2 forcing was used when simulating power extraction. The fetch of each energy extraction zone ℓ (i.e. the longitudinal distance between the site inlet and outlet parallel to the direction of flow over which added drag was applied − shown in Fig. 3) was determined based on the distribution of mean ambient kinetic power to cover the most energetic regions where tidal energy development is most likely to be carried out. The average extracted power was calculated by integrating over the zone area and with respect to time t, where T is the duration of the repeating M_2 tidal cycle equal to 12.41 h [6]:

$$P = \frac{1}{T} \int\limits_0^T \left(\int \int\limits_{A_z} \rho C_e |u|^3 dA \right) dt \qquad (10)$$

The equivalent added drag coefficient was increased incrementally to simulate more turbines (i.e. to increase array density defined as the ratio of total swept area of all turbines to the array plot area) until the total energy dissipated by the added drag reached a maximum and any further increase in drag caused a reduction in average extracted power. A summary of the simulations undertaken to validate the model and quantify power extraction are summarised in Table 2.

3. Model validation

3.1. Tidal elevations

Driven by M_2, S_2, N_2, K_2, K_1, O_1,P_1, Q_1 and M_4 forcings, a 30 day simulation was run to generate validation datasets for M_2 and S_2 elevations and velocities. Surface elevation time series were extracted from 13 locations around the domain (Fig. 2) including six locations around the Channel Islands (Alderney, Guernsey, Jersey, Sark, Cherbourg and St. Malo). Tidal harmonic analysis was conducted using the Matlab package T-tide [26] to estimate the amplitude and phase of the M_2 and S_2 constituent at each location from the free surface elevation time series', which was then compared with data from the Tidal Analysis Software Kit (TASK) [27] and Admiralty Tide Chart data [28].

The results from the simulation undertaken to validate the model are shown in Table 3. These show that nine out of thirteen ports were within 10% of real M_2 and S_2 amplitudes and 10° of real M_2 and S_2 phases, including all six ports around the Channel Islands. The region with the greatest discrepancy in tidal amplitude

Table 3
Percentage differences between modelled and real-world (admiralty chart [28]) M_2 and S_2 amplitudes and phases at 13 ports around the English Channel Model domain (locations shown in Fig. 2) using tidal harmonic analysis.

Port	Amplitudes		Phases	
	M_2 error (m)	S_2 error (m)	M_2 error (°)	S_2 error (°)
Alderney	−0.12 (−7%)	−0.06 (−8%)	+5	+9
Jersey	−0.29 (−9%)	+0.01 (+7%)	0	+5
Guernsey	−0.4 (−10%)	−0.11 (−10%)	+6	+6
Sark	−0.16 (−9%)	+0.03 (+3%)	+10	+10
Cherbourg	−0.04 (−2%)	+0.04 (+6%)	−4	+3
St. Malo	−0.34 (−9%)	−0.13 (−5%)	0	−1
Newlyn	+0.11 (+6%)	−0.05 (−8%)	+9	+9
Weymouth	+0.14 (+23%)	+0.04 (+14%)	−9	0
Bournemouth	+0.35 (+84%)	+0.11 (+56%)	+14	+4
Newhaven	+0.25 (+11%)	+0.08 (+12%)	+21	+22
Dover	+0.17 (+8%)	+0.07 (+10%)	+19	+22
Dunkirk	−0.38 (−18%)	+0.11 (18%)	+75	+19
Le Havre	+0.28 (+10%)	+0.07 (+7%)	+6	+7

is along the south coast of England, where amplitudes are significantly smaller than at other ports. For example, tidal amplitudes at Bournemouth and Weymouth are 0.42 m and 0.59 m respectively, in comparison with 1.87 m at Cherbourg and 1.72 m at Newlyn. In these shallower regions the amplitude is a greater proportion of the total depth, making free surface elevation more sensitive to drag due to bottom friction, which removes a greater proportion of the propagating tidal energy, causing a reduction in amplitude [29]. Furthermore, any small absolute error will be most noticeable in shallower regions where the error is a greater proportion of the total depth. Amplitude and phase results shown in Table 3 were obtained with a uniform Nikuradse drag coefficient over the domain of $C_b = 0.025$. Further refinement of the model in this region was not deemed necessary since the significant distance to the Channel Islands meant it had little to no impact on the validation results in the area of interest.

3.2. Tidal stream velocities

Data from three AWAC deployments (locations shown in Fig. 4) commissioned by the Alderney Renewable Energy (ARE) in 2009 were used to validate tidal stream velocities in Alderney Race. The AWACs were deployed for a minimum period of 30 days.

Fig. 5 shows results for M_2 and S_2 constituent major axis amplitudes, phases and inclinations obtained from the English Channel model compared with field measurements.

Errors at locations a (Fig. 5a) and c (Fig. 5c) are likely to be caused by the large clockwise eddies shed off the North East tip of Alderney during the ebb tide (shown in Fig. 4), creating a complex

Table 2
Summary of the 8 scenarios simulated using the English Channel model. Scenario 1 is for validation, quantifying the distribution of mean flow velocities and kinetic power. Scenarios 2−8 are the energy extraction cases considered at sites in the Channel Islands.

| Scenario	Energy extraction location	Objective
1	Not applicable, ambient flow only	Model validation/Quantify distribution of mean flow velocities and kinetic power at sites around the Channel Islands/Obtain elevation data to input into an analytical model (Equation (12)) for power potential.
2	Alderney Race	Quantify the maximum average power potential, as well as a realistic level of power extraction and array density described by Equations (7) and (8).
3	Casquets	As above (Scenario 2).
4	Big Roussel	As above (Scenario 2).
5	Alderney Race + Casquets	Quantify level of interaction between sites based on upper bound levels of power extraction and realistic levels of energy extraction and array density described by Equations (7) and (8) for the 2 sites.
6	Alderney Race + Big Roussel	As above (Scenario 5) for the 2 sites.
7	Casquets + Big Roussel	As above (Scenario 5) for the 2 sites.
8	Alderney Race + Casquets + Big Roussel	As above (Scenario 5) for the 3 sites.
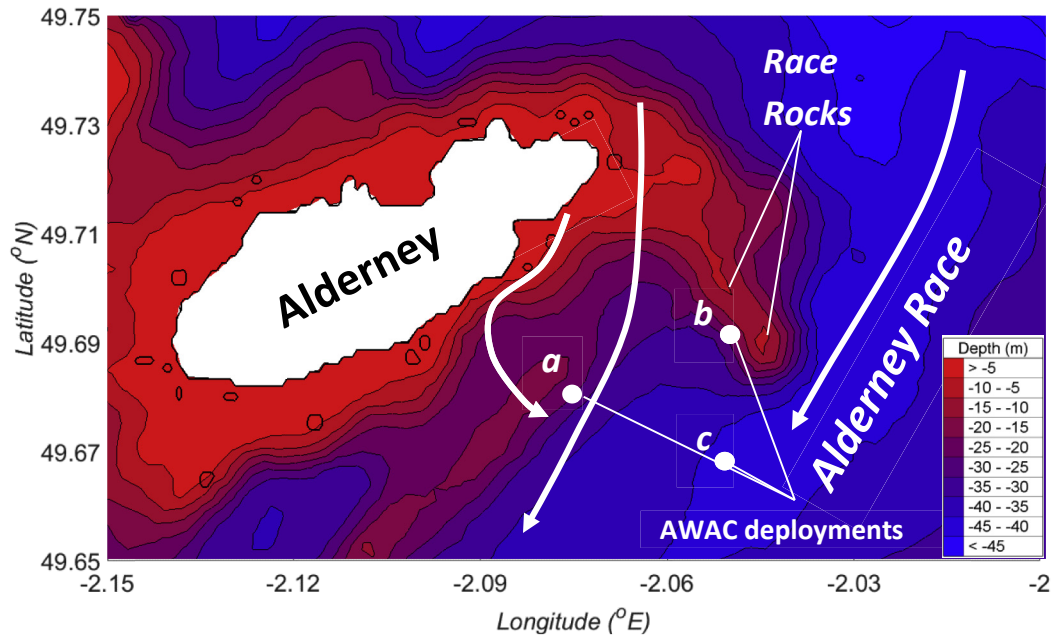
Fig. 4. Location of three AWAC deployments (*a,b* and *c*) in Alderney Race. Arrows show the direction of the dominant ebb tide and the eddy shed off the North East tip of Alderney. The location of Race Rocks is also shown.
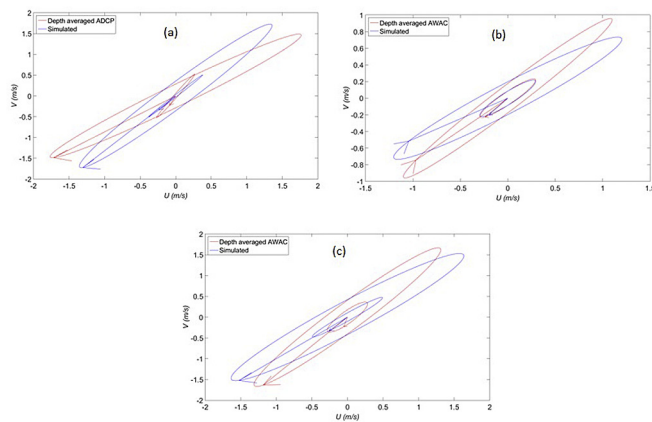

Fig. 5. M_2 and S_2 tidal stream ellipses for (a) AWAC deployment a (b) AWAC deployment b and (c) AWAC deployment c. Locations of AWAC deployments shown in Fig. 4.

flow pattern in this region. It was shown in Ref. [30] that the angular velocity and directional propagation of this eddy is sensitive to the magnitude to sea bed drag coefficient C_b.

AWAC *b* is in close proximity to Race Rocks (shown in Fig. 4), two tower like rock formations in close proximity to one another that accelerate flow through and around them, creating strong jet flows during ebb tide. Results from Fig. 5b (summarised in Table 4) show that the model is capturing the flow dynamics in this region well,

Table 4
Differences in M_2 and S_2 major axis, phases and inclination between simulated results and AWAC data at three locations in Alderney Race.

AWAC	Major axis amplitude difference (%)	Phase difference (°)	Inclination difference (°)
a	10/7	9/17	−12/−10
b	4/2	−1/−13	−10/2
c	−5/−53	3/9	−9/−9

where the M_2 and S_2 major axis amplitudes show agreement within 5%, phases within 13% and inclinations within 10%.

Validation results are summarised in Table 4, showing all M_2 and S_2 constituent major axis amplitudes, phases and inclinations obtained from the English Channel model compared with field measurements. With the exception of the S_2 major axis amplitude at location *c*, all M_2 and S_2 major axis amplitudes and phases lie within 15% of field measurements. Phases and inclinations also show reasonable agreement, with all results excluding the S_2 phase at location *a* lying within 15° of the true values.

4. Results and discussion

4.1. Ambient flow

The model was run in the ambient case for 31 days, plus 24 h to allow the model to spin up from still water conditions. In total nine tidal constituents were used to force each open boundary (M_2, S_2, N_2, K_2, K_1, O_1, P_1, Q_1 and M_4). Ambient flow results were used to estimate the distribution in mean kinetic power, a metric commonly used for quantifying a resource [12,31]:

$$P = \frac{1}{T} \sum_{i=1}^{T} \frac{1}{2} \rho U_i^3 \qquad (11)$$

Fig. 6 shows the contour plot of mean kinetic power density distribution, which was used for approving/discarding sites in the Channel Islands based on assumptions used in Ref. [12] where it is estimated that for 'reasonable project economics' using first generation turbine devices, mean kinetic power density should exceed 2.5 kW/m^2. In our simulation, the highest kinetic power density is seen in Alderney Race, where in the shallower faster waters of the East Race kinetic power density exceeds 13.5 kW/m^2 and the mean flow exceeds 2.5 kW/m^2 over an area of 93 km^2. Depths across the majority of Alderney Race exceed 15 m and never go above 50 m, making it geometrically suitable to house 1st and 2nd generation devices.
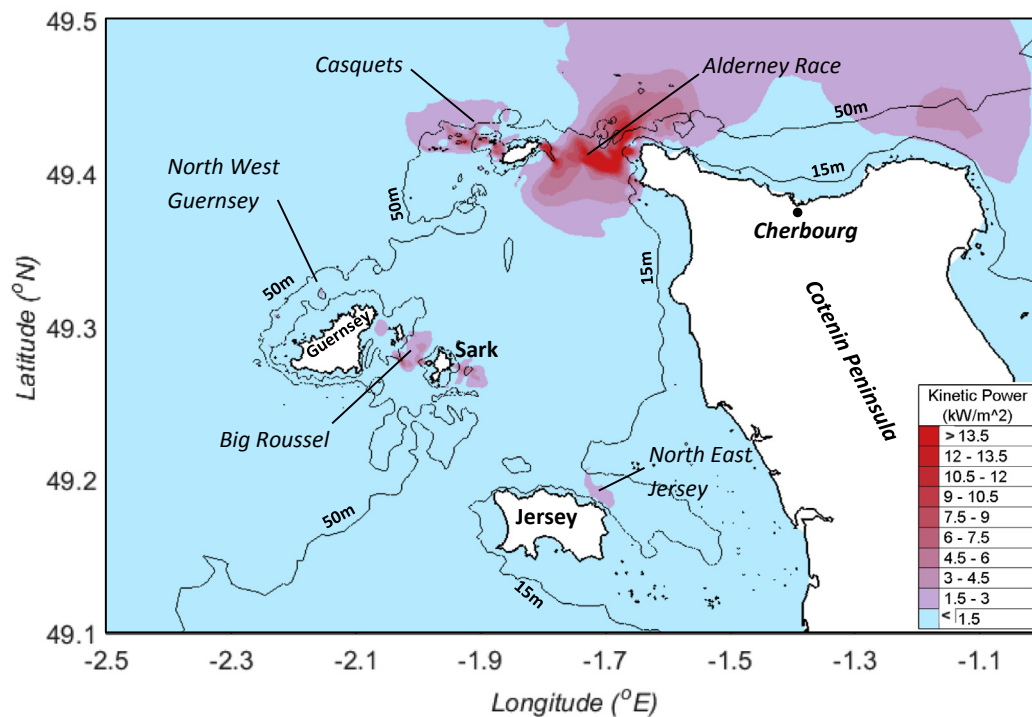
Fig. 6. Mean kinetic power density distribution around the Channel Islands, with 50 m and 15 m depth contours also shown.

As shown in Fig. 6, both Casquets and Big Roussel also exhibit mean power densities greater than 2.5 kW/m^2, however in both cases the area over which this is true is 7 km^2 and 14 km^2 respectively, significantly smaller compared to that of the Alderney Race (summarised in Table 5). The maximum kinetic power density at Casquets and Big Roussel was 7 kW/m^2 and 5 kW/m^2 respectively.

In Fig. 6 we show a 10 km^2 region where mean kinetic power density exceeds 1.5 kW/m^2 in North East Jersey, potentially making it a viable option in the future as costs related to aspects such as manufacturing, installation and operation and maintenance reduce. However the mean kinetic power density at sites around North West Guernsey and North East Jersey identified in Ref. [1] do not exceed 2.5 kW/m^2 and are therefore not considered further in this study.

These result are in contrast to past assessments covered in Table 1 ([2,3,32,5,33]) that assume the velocities are high enough for tidal energy development over areas of up to 58 km^2 in North East Jersey, 366 km^2 in North West of Guernsey, 90 km^2 in Big Roussel and 215 km^2 in Casquets. In Table 5 we summarise the areas over which the mean kinetic power exceeds 2.5 kW/m^2 within

depths of 15−50 m at each site and also give a comparison with previous studies. In general, the areas identified in our work are significantly smaller than previous studies.

We feel these results are more robust as, unlike previous studies, we have used higher resolution flow data and imposed stricter limits on the acceptable mean velocities. For the same data and limits, the exception to this is Alderney Race, where the estimated potential development area is approximately 30% greater than previously estimated [5,33]. There are two small regions either side of Big Roussel that also exhibit high kinetic power density, however they occur in shallow waters and are therefore not consider further in this study.

4.2. Maximum average power potential

In estimating the maximum average power potential, drag was applied uniformly to the energy extraction zones shown in Fig. 3. These zones were sized and positioned to overlay regions where the mean kinetic power density exceeds 2.5 kW/m^2. In regions close to coastlines, the energy extraction zones cover shallow waters unsuitable for energy extraction by turbines. This was included

Table 5
Summary of area considered in this study over which distribution of mean kinetic power density exceeds 2.5 kW/m^2 at Alderney Race, Casquets, Big Roussel, North West Guernsey and North East Jersey in comparison with previous studies (in Table 1).

Site	This Study	Previous studies	
	Area exceeding 2.5 kW/m^2 in depths of 15−50 m (km^2)	Area considered to be energetic (km^2)	Sources
Alderney Race	93	65−102	ETSU [3], European Commission [4], Bahaj et al. [5], Myers et al. [33]
Casquets	7	61−215	ETSU [3], European Commission [4], Black and Veatch Phase II [2]
Big Roussel	14	90	ETSU [3]
North West Guernsey	0	221−366	ETSU [3], European Commission [4]
North East Jersey	0	20−58	ETSU [3], European Commission [4], Black and Veatch Phase II [2]

Table 6
Comparison between this work and published data of the estimated of maximum average power potential of different high potential sites for tidal power extraction. The table includes our results for Alderney Race, Casquets and Big Russel within the realistic bounds of seabed roughness coefficient $C_b = 0.013-0.052$.

Site	Estimated maximum average power potential (GW)	Boundary forcing
Past assessments of other sites		
Minas Passage, Canada [8]	5.7	$M_2, S_2, N_2, K_2, K_1, O_1, P_1, Q_1, M_4$
Pentland Firth, Scotland [6]	3.75	M_2 only
Johnstone Strait, Canada [9]	1.3	M_2 only
Masset Sound, Canada [10]	*0.08*	M_2 only
This work		
Alderney Race	4.7–5.5	M_2 only
Casquets	0.43–0.51	M_2 only
Big Roussel	0.22–0.26	M_2 only

in our analysis to limit flow acceleration around the energy extraction zones within each site, and follows the same methodology as in literature for the Pentland Firth [6], Minas Passage [8] and Masset Sound [10] to allow direct comparison between sites. The model was run with M_2 boundary forcing for 36.41 h, made up of 24 h for spin up and one semi diurnal tidal cycle for analysis.

4.2.1. Alderney Race

As the drag coefficient C_e applied uniformly over the energy extraction zone in Alderney Race is increased from zero, the average free surface elevation difference across the energy extraction zone ($Z_{in}-Z_{out}$) increases, as shown in Fig. 7. This increases the hydrostatic force driving flow through the energy extraction zone to oppose the added drag from C_e. The increase in drag coefficient C_e also results in a reduction in the average volume flux through the energy extraction zone (also shown in Fig. 7) due to the enhanced hydraulic resistance from C_e so that flow diverts away from Alderney Race (this flow diversion is discussed further in §4.3 and §4.4). Since extracted power is the product of the elevation drop across the energy extraction zone ($Z_{in}-Z_{out}$) and the volume flux through the energy extraction zone (Q), as C_e increases, the level of extracted power is dependent on the rate of change of both Q and ($Z_{in}-Z_{out}$) with respect to C_e. I.e. As C_e increases, if the increase in elevation drop dominates the reduction in volume flux, extracted power will

increase, but if the reduction in volume flux supresses the increase in elevation drop, extracted power will decrease. For the case of Alderney Race the maximum average power potential was 5.1 GW, as shown in Fig. 8.

To validate the English Channel model a uniform seabed roughness coefficient $C_b = 0.025$ was applied over the whole domain, as discussed in §3. However, in reality seabed roughness coefficient C_b varies spatially (due to spatial distribution of bed roughness properties throughout the domain), directionally (due to the bi-directional nature of the tides) and temporally (due to changes to bed morphology from scour and sediment dynamics). In Ref. [34] it was shown that the level of power extraction from tidal turbines is sensitive to small changes in sea bed roughness coefficient C_b, where if seabed drag coefficient is increased, more power is extracted by the bed, reducing the power extracted by the turbines. For this reason, simulations were re-run for seabed roughness coefficients within physically realistic bounds by assuming the roughness height d_{90} (Equation (6)) does not exceed 2% of the depth h but is greater than 0.005% of the flow depth, resulting in a range of C_b of $0.013-0.052$ obtained from Equations (5) and (6).

Error bars in Fig. 8 show the sensitivity of extracted power to sea bed drag coefficient C_b, which for the peak average extracted power is approximately 15%. In general, as bed friction coefficient was increased to $C_b = 0.052$, the extracted power decreased because more power is extracted by the seabed.

To provide more resilience in the results, the English Channel model was run for an ambient case without power extraction with M_2 forcing. Using Equation (12), an estimate of the maximum average power potential was obtained from the theory developed in Ref. [35], where γ is a coefficient ranging between 0.16 and 0.24 depending on the phase difference between the flow rate and the driving head [26], ρ is water density, g is acceleration due to gravity, a_0 is the amplitude difference between the two ends of the channel and Q_{max} is the maximum volume flux through the channel in the undisturbed case.

$$P_{max} = \gamma \rho g a_0 Q_{max} \qquad (12)$$

This yielded a maximum average power of 4 GW, using a peak flow in the undisturbed state, $Q_{max} = 1.08 \times 10^6 \, \text{m}^3/\text{s}$, $\gamma = 0.22$ and a head difference $a_0 = 1.13$ m. The head difference was taken from points located 25 km from the narrowest constriction of the Race
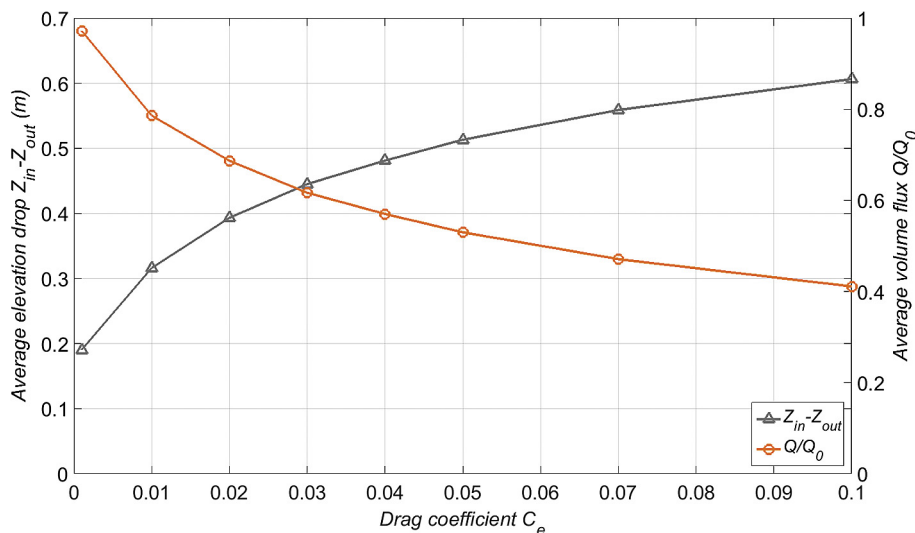

Fig. 7. Reduction in average volume flux (Q/Q_0) through Alderney Race and increase in elevation difference across Alderney Race ($Z_{in}-Z_{out}$) as a result of increased drag coefficient, C_e applied uniformly over the energy extraction zone.
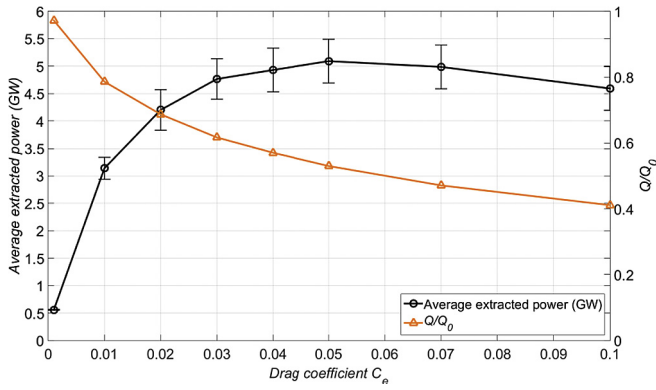
Fig. 8. Average extracted power from Alderney Race over an M_2 tidal cycle with decreasing flow rate as a result of increased drag coefficient, C_e applied uniformly over the energy extraction zone. Error bars show the average extracted power within the realistic limits of $C_b = 0.013-0.052$.

(i.e. so that the two points were located 50 km apart from each other). The phase lag of flow rate behind the dynamic head was 48°.

The estimate for the maximum average power potential obtained using Equation (12) was within 20% of the estimate from the numerical model using the distributed drag approach. Error in this analytical estimate arises from the dynamic head difference a_0, which does not remain unaffected by power extraction as assumed by Equation (12) (a_0 increases when a drag is applied over the energy extraction zones). Closer agreement would be possible using points located further than 25 km away from Alderney Race to estimate the head drop given that it was found that power extraction did have an effect on free surface elevations at the locations used, however the difference was found to be less than 5%. This was deemed to be acceptable given that other simplifications in the analytical approach are likely to contribute a significant error to the maximum average power potential result. For example important flow features such as exit losses (resulting from flow separation) and Coriolis are not considered.

To add more constituents, [29,35] provide a solution with amplitudes $a_1, a_2,..,a_i$, where the solution to Equation (12) is multiplied by $x = 1 + \alpha(r_1^2 + r_2^2 + ... + r_i^2)$, where α is a fraction between 9/16 and 1 depending on the basic dynamic balance and $r_i = a_i/a$ is the ratio of the amplitude of the dynamic head of constituent i to the dynamic head of the dominant constituent. To add the S_2 constituent, $x = 1.1$ was used based on $r_1 = 0.45$ obtained from the

numerical model, giving a maximum average power potential of approximately 4.4 GW.

4.2.2. Casquets

The same procedure was carried out for Casquets, giving an estimated maximum average power potential with $C_e = 0.02$ of 0.47 GW, which is approximately 10% of Alderney Race (Fig. 9). At this upper bound, the reduction in volume flux was 42%, the same fraction reduction as for Alderney Race and in line with analytical results [9]. Our estimated result of 0.47 GW is approximately double the value obtained in Ref. [36] where a 2D hydrodynamic models of generic tidal regimes such as tidal streams were developed to simulate the large scale impact of hypothetical levels of power extraction. However Casquets is unlikely to be fully representative of the idealised case, especially as bathymetry varies significantly across the site and there are alternative channels for the flow to take into the English Channel and into Alderney Race. The variation in the results with seabed roughness coefficient C_b were approximately within the same error bounds as for Alderney Race, where the maximum average power potential showed a 13% variation.

4.2.3. Big Roussel

The estimated maximum average power potential of Big Roussel was 0.24 GW, approximately 5% of Alderney Race and 50% of Casquets. This gave a reduction in volume flux through the channel of 43% with $C_e = 0.09$ (Fig. 10). At this upper bound the sensitivity to sea bed friction drag C_b was also 15%.

For comparison, Table 6 summarises our estimated maximum average power potential results for the three sites considered here along with four other well-known studies at other tidal sites in literature. These results should also be compared with outcomes from previously published work undertaken for the Channel Islands sites given in Table 1. Our results indicate that Alderney Race has the greatest potential in the Channel Islands which is significant given that it is approximately 136% that of the maximum average power potential estimated for the Pentland Firth in Scotland [6]. Casquets and Big Roussel are significantly lower, which is unsurprising given that these two sites are considerably smaller and in general have a lower kinetic power density distribution, as was shown in Fig. 6.

The effect of varying the fetch l of each energy extraction zone on the magnitude of the maximum average power potential was investigated. It was found that by increasing the zone fetch l, the drag coefficient C_e required to obtain the maximum average power potential decreased. However, the magnitude of the maximum
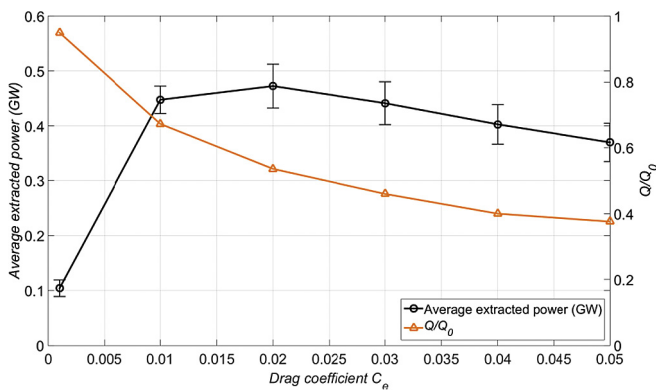

Fig. 9. Average extracted power from Casquets over an M_2 tidal cycle with decreasing flow rate as a result of increased drag coefficient C_e applied uniformly over the energy extraction zone. Error bars show the average extracted power within the realistic limits of $C_b = 0.013-0.052$.

Fig. 10. Average extracted power from Big Roussel over an M_2 tidal cycle with decreasing flow rate as a result of increased drag coefficient C_e applied uniformly over the energy extraction zone. Error bars show the average extracted power within the realistic limits of $C_b = 0.013-0.052$.
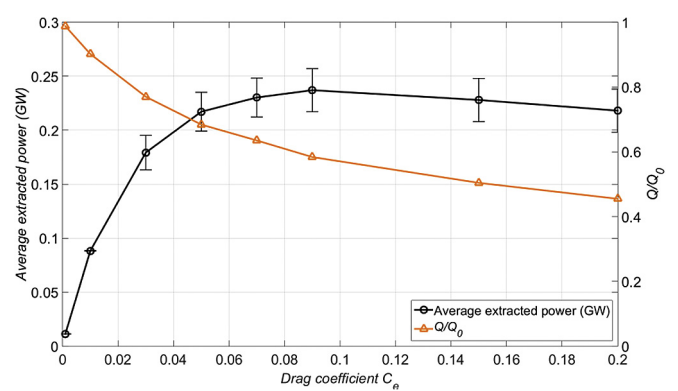
Table 7
Maximum average extracted power for all seven scenarios (scenarios first presented in Table 2) using Alderney Race with $C_e = 0.05$, Casquets with $C_e = 0.02$ and Big Roussel with $C_e = 0.09$ and seabed drag coefficient $C_b = 0.025$.

Scenario	Combinations	Power potential (GW)			
		Alderney Race	Casquets	Big Roussel	Total (GW)
2	Alderney Race	5.10	–	–	5.10
3	Casquets	–	0.47	–	0.47
4	Big Roussel	–	–	0.24	0.24
5	Alderney Race + Casquets	5.28	0.84	–	6.12
6	Alderney Race + Big Roussel	5.03	–	0.21	5.24
7	Casquets + Big Roussel	–	0.56	0.23	0.79
8	Alderney Race + Casquets + Big Roussel	5.24	1.02	0.20	6.46

average power potential did not change (within 5%). This was also found to be the case for a considered narrow zone of turbines spanning the width of the entrance to Minas Passage compared with a drag distributed over the entire area of the channel [8]. In their work it was shown that for a given geometry and forcing, the product of the energy extraction zone fetch l and the effective added array drag coefficient C_e used to obtain the maximum average power potential remains constant [5].

4.3. Interaction

The three sites considered here are in relatively close proximity, especially Alderney Race and Casquets, separated only by the 3 km wide island of Alderney, whilst Big Roussel is approximately 40 km from Alderney Race and Casquets. Therefore, power extraction at each site is likely to affect the surrounding flow dynamics, hence altering the total power potential of each neighbouring site. Such interactions were quantified using the methodology originally adopted by Draper at al. [6] in which simultaneous power extraction scenarios were simulated (scenarios listed in Table 7). For all scenarios, the upper bound (optimum value) drag coefficient C_e for each of the individual sites was used.

Simultaneous power extraction at Alderney Race and Casquets (Scenario 5) gives a 79% increase in the estimated maximum average extracted power at Casquets and a 10% increase in the overall total power extracted in comparison to power extraction at Alderney Race and Casquets simulated separately (Scenarios 2 and 3). Power extraction at Alderney Race (Scenario 2) causes flow diversion around Alderney giving a 25% increase in volume flux through Casquets and an increase in

average head drop across Casquets of 0.03 m in comparison with power extraction at Casquets only (Scenario 3). The increase in mean velocities through Casquets due to power extraction at Alderney Race is shown in Fig. 11a. The figure shows the difference between the mean velocity distribution for power extraction at Alderney Race and Casquets together (Scenario 5) and power extraction at Casquets only (Scenario 3). Red regions show areas of enhanced mean velocities due to power extraction in Alderney Race, which occurs in and around the Casquets energy extraction zone.

The results in Fig. 11a highlight the inter-dependent nature of power extraction when both Alderney Race and Casquets are exploited, where power extraction at the Alderney Race has a significant impact on the resource at Casquets. This is encouraging as it means that the greater the development in Alderney Race, the more energetic the resource at Casquets becomes.

The reduction in mean velocities through Big Roussel as a result of power extraction at Alderney Race and Casquets is shown in Fig. 11b. This corresponds to a 17% reduction in extracted power at Big Roussel as a result of power extraction at Alderney Race and Casquets (Scenario 8) when compared to that at the Big Roussel in isolation (Scenario 4). This is attributed to the fact that on the dominant ebb tide, power extraction at Alderney Race and Casquets, which are both upstream of Big Roussel, cause flow diversion around the Channel Islands, giving a 2.5% reduction in volume flux through Big Roussel in comparison with the case of power extraction at Big Roussel only (Scenario 4).

The dependencies listed in Table 7 have major implications for the exploitation of the sites. For a developer that leases a plot in Casquets or Big Roussel, failing to consider the effects of power
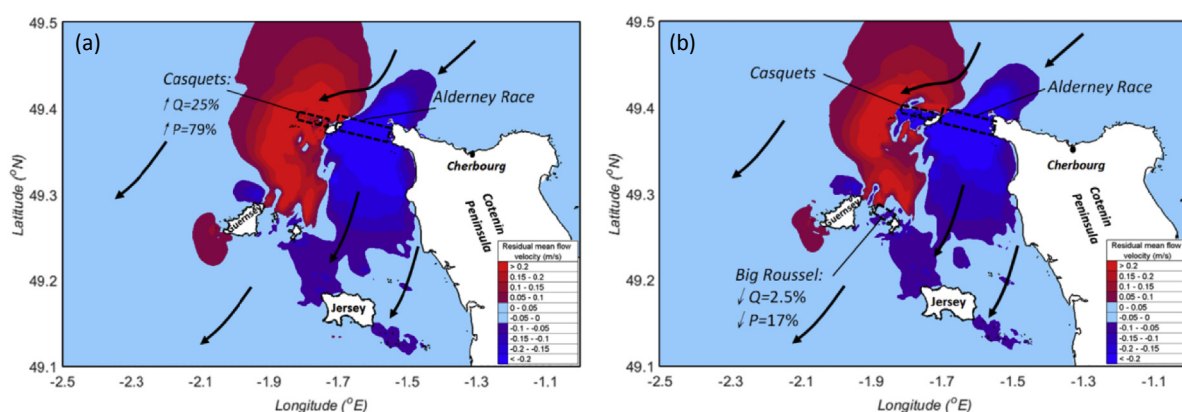

Fig. 11. Mean velocity distribution difference plot between (a) the case of upper bound power extraction at Casquets (Scenario 3 described in Table 7) and power extraction at Alderney Race and Casquets (Scenario 5 described in Table 7) (b) the case of upper bound power extraction at Big Roussel only (Scenario 4 described in Table 7) and power extraction at Alderney Race, Casquets and Big Roussel (Scenario 8 described in Table 7). Arrows show the direction of the dominant ebb tide and flow diversion around Alderney Race into Casquets.

Table 8
Estimated equivalent longitudinal and lateral (tip to tip) spacing between devices to achieve maximum average power potential at each individual site, with corresponding array density obtained using Equations (7) and (8).

Site	Optimum C_e	Corresponding array density λ	Equivalent lateral spacing in device diameters (D)	Equivalent longitudinal spacing in device diameters (D)
Alderney Race	0.05	0.125	1	4
Casquets	0.02	0.050	1	10
Big Roussel	0.09	0.225	1	2

extraction at Alderney Race (the neighbouring inter-dependant site) on flow within the leased plot will ultimately lead to an over/under estimation of extracted power. Regulators and developers should be aware of this so that a coherent development is planned for to account for such impacts. However, currently to the authors knowledge, there is no clear regulation that takes into account such dependency. We hope that this work will provide the evidence to support the development of regulations that take into account the interdependencies between neighbouring tidal sites.

4.4. Realistic array drag and power from sites

In reality the zone drag coefficient C_e is limited by the physical constraints of the turbines and turbine spacing. The equivalent added drag from tidal turbines can be estimated using Equations (7) and (8). Table 8 gives an approximate longitudinal spacing for the optimum effective zone drag coefficient C_e used to obtain the maximum average power potential at each site using Equations (7) and (8) and assuming a lateral spacing (tip to tip) of 1 diameter. This lateral spacing was chosen as it is likely to be close to the limit for which devices can physically be installed next to each other. In Equation (8) a turbine drag coefficient of $C_D = 0.8$ was used [24].

Table 8 shows that to achieve the maximum average power potential at Alderney Race and Big Roussel, very high turbine densities are required. For these two sites the flow is constricted due to the positioning of coastlines so that an increase in distributed drag results in an increase in head drop across the zone, resulting in an increase in extracted power. Such high packing densities are unlikely to ever be realised as turbines will be in the near wake of upstream devices [37], severely diminishing efficiency. For the device spacing shown in Table 8, to extract maximum power in Casquets requires the least densely packed array. This is because Casquets is open to the English Channel so is the least constricted site, allowing flow to divert around the energy extraction zone more easily with an increase in distributed drag, resulting in a reduction in volume flux through the energy extraction zone. A longitudinal spacing of ten diameters is a more realistic packing density that will allow wakes to at least somewhat

recover between each row, however the extent of wake recovery within arrays is still unclear.

Further simulations were conducted using a value of added drag based on the assumption that turbines have one diameter lateral spacing (tip to tip), and ten diameter longitudinal spacing, giving $C_e = 0.015$ and a uniform array density $\lambda = 0.038$ (using Equations (7) and (8)). This drag was applied over the same energy extraction zones as used before. The results are presented in Table 9, showing the reduction in estimated maximum average power potential in comparison with the maximum average power potential at each site from §4.2 (column 8).

The results show that the reduction in extracted power relative to the maximum (upper bound) average power potential differs for each site. For Casquets, the maximum average power potential ($P = 0.47$ GW) was achieved with a relatively low added drag of $C_e = 0.02$ because flow easily diverted into the English Channel as drag was added. This upper bound drag coefficient $C_e = 0.02$ used for estimating the maximum average power potential is close to the realistic value of $C_e = 0.015$ used to obtain the results in Table 9. For added drag in the range $0.01 < C_e < 0.03$, Casquets power curve shown in Fig. 9 is relatively flat so that there is no change in extracted power between the maximum and realistic case. This is demonstrated in Fig. 12, which compares the change in average extracted power at Casquets and Alderney Race for the maximum and realistic cases.

At Alderney Race the maximum average power potential (upper bound; $P = 5.1$ GW) was obtained with a significantly higher added drag coefficient $C_e = 0.05$ (Fig. 8), because of the more constricted nature of the site and higher ambient velocities. Therefore when C_e was reduced to the more realistic case ($C_e = 0.015$, Fig. 12), there was a significant reduction in extracted power of 24%. The greatest drop in average extracted power was 50% at Big Roussel (Scenario 4), where the difference between optimum C_e ($=0.09$) and the realistic level applied here ($C_e = 0.015$) is greatest.

Site interdependencies using the realistic value of C_e are also quantified in Table 9 (Scenarios 5—8), and these should be compared with Table 7 for the upper bound cases (results repeated in column 7 of Table 9).

Table 9
Average extracted power for Scenarios 2—8 (first presented in Table 2) using Alderney Race, Casquets and Big Roussel with an added drag coefficient, $C_e = 0.015$. Column 6 gives the average extracted power for the revised C_e, column 7 gives the maximum average power potential for the optimum C_e given in Table 7 and column 8 shows the % reduction in power potential between the two cases. Column 9 shows the change in mean volume flux through each site for the realistic cases, given as a ratio of the volume flux with power extraction (Q) and without power extraction from the ambient flow using Scenario 1 (Q_0).

| Scenario (1)	Sites and sites combinations (2)	Realistic average extracted power (GW)				Maximum extracted power (GW) (from Table 7) (7)	Change % (8)	Q/Q_0 (9)
		Alderney Race (3)	Casquets (4)	Big Roussel (5)	Total for site(s) (6)			
2	Alderney Race	3.86	—	—	3.86	5.10	−24%	0.73
3	Casquets	—	0.47	—	0.47	0.47	−0%	0.56
4	Big Roussel	—	—	0.12	0.12	0.24	−50%	0.89
5	Alderney Race & Casquets	4.05	0.79	—	4.84	6.12	−21%	0.69 & 0.61
6	Alderney Race & Big Roussel	3.87	—	0.12	3.99	5.24	−23%	0.75 & 0.90
7	Casquets & Big Roussel	—	0.49	0.12	0.69	0.79	−13%	1.05 & 0.90
8	Alderney Race, Casquets & Big Roussel	4.01	0.78	0.11	4.90	6.45	−24%	0.71 & 0.60 & 0.85
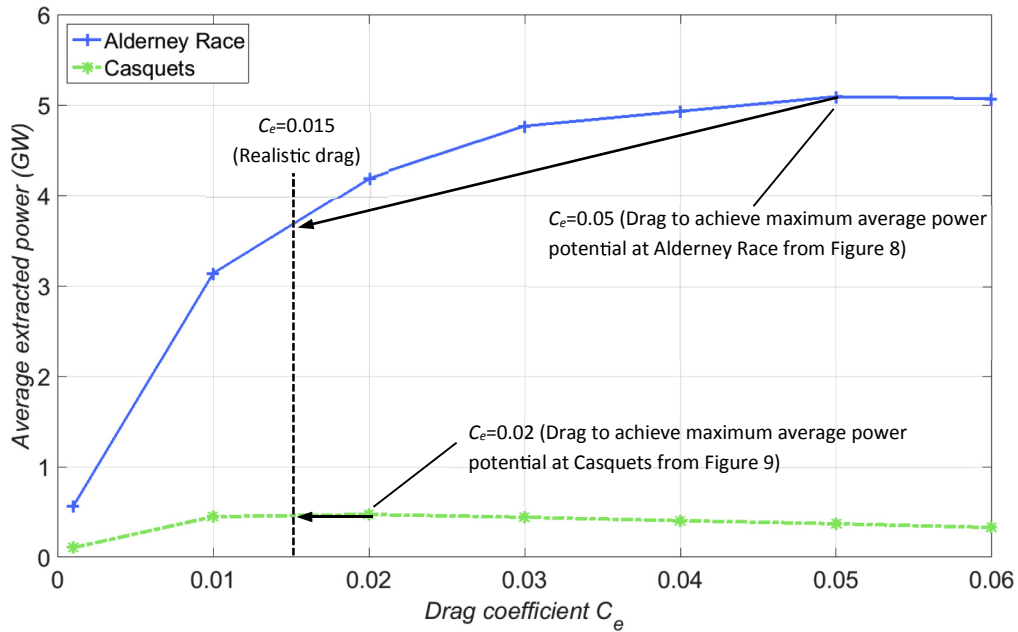
Fig. 12. Average extracted power from Alderney Race and Casquets over an M_2 tidal cycle as a result of increased drag coefficient C_e applied uniformly over each energy extraction zone. Graph illustrates the reduction in mean extracted power when comparing the upper bound cases against a realistic level of $C_e = 0.015$ at both sites.

4.5. Available power

The available power is defined as the fraction of the extracted power that is removed by ideal tidal turbines for electrical power production [6], so is lower than the power potential which considers the extracted power only. The available power for electrical power production was estimated based on a power coefficient $C_p = 0.3$ using Equation (13). These results quantify the electrical power that could be generated by positioning turbines within the energy extraction zones located in Alderney Race, Casquets and Big Roussel with a uniform array density $\lambda = 0.0375$, corresponding to $C_e = 0.015$.

$$P = \frac{\lambda}{2}\frac{1}{T}\int_0^T \left(\int\int_{A_z} \rho C_p |u|^3 dA \right) dt \qquad (13)$$

Results for available power, obtained using Equation (13), are presented in Table 10. Column 7 shows the realistic *extracted* power obtained previously in §4.4 for comparison. As would be expected, the available power is significantly lower than the extracted power to account for the coefficient of power in Equation (13), as well as the swept area of the rotors. In general the available power estimated here is 37% of the realistic extracted power. This analysis shows that if the entire width of each site is developed the total average available power at all three sites from the M_2 tide is 1.83 GW, with 82% from Alderney Race, 16% from Casquets and 2% from Big Roussel. Given that results presented here were obtained with M_2 forcing only, the inclusion of additional constituent forcings would increase estimates for extracted and available power, which is the subject of ongoing work.

4.6. Change in flow dynamics

Fig. 13a shows the change in mean velocity distribution due to power extraction at Alderney Race (Scenario 2) in comparison to the ambient flow (Scenario 1). The realistic level of drag used in §4.4 was applied uniformly over the energy extraction zone in Alderney Race, causing flow to divert around Alderney and through Casquets, giving an increase in mean flux through Casquets of $Q/Q_0 = 1.09$ and a reduction in volume flux through Alderney Race of $Q/Q_0 = 0.73$. Power extraction at Alderney Race (Scenario 2) has no significant impact on the velocities at Big Roussel, where velocities match those in the ambient case, giving the same mean volume flux through Big Roussel (i.e. $Q/Q_0 = 1$). This may change with the inclusion of additional boundary forcings which increases velocities within the Channel Islands, hence increasing the magnitude of the force exerted on the flow at the energy extraction zone in Alderney Race and increasing the magnitude of bypass velocities around Alderney into Casquets and down into Big Roussel.

When power is extracted at Alderney Race *and* Casquets together (Scenario 5), power extraction at Alderney Race causes an increase in power extracted at Casquets in comparison to power extracted at Casquets only (Scenario 3) of 0.32 GW, an increase of 68%. This results in an increase in total extracted power (at both sites) of 12% compared with power extraction from the individual sites simulated separately (Scenarios 2 and 3). This is a similar finding to the upper bound case, emphasising the need for regulators and developers to account for the constructive impact from dual development at Alderney Race and Casquets when designing turbine layouts, as it will lead to improved energy yield, making it a more attractive proposition.

Fig. 13b shows the change in mean velocity distribution due to power extraction at Casquets in comparison to the ambient flow. The increased drag applied uniformly over the energy extraction zone in Casquets diverts flow into the English Channel and through Alderney Race, shown by regions of enhanced mean velocity in Fig. 13b. The added drag applied at Casquets gives a small increase in mean flux through Alderney Race of $Q/Q_0 = 1.02$ and a reduction in volume flux through Casquets of $Q/Q_0 = 0.56$. This high reduction in volume flux through Casquets is because Casquets is the least constrained site, so flow is easily diverted into the English Channel
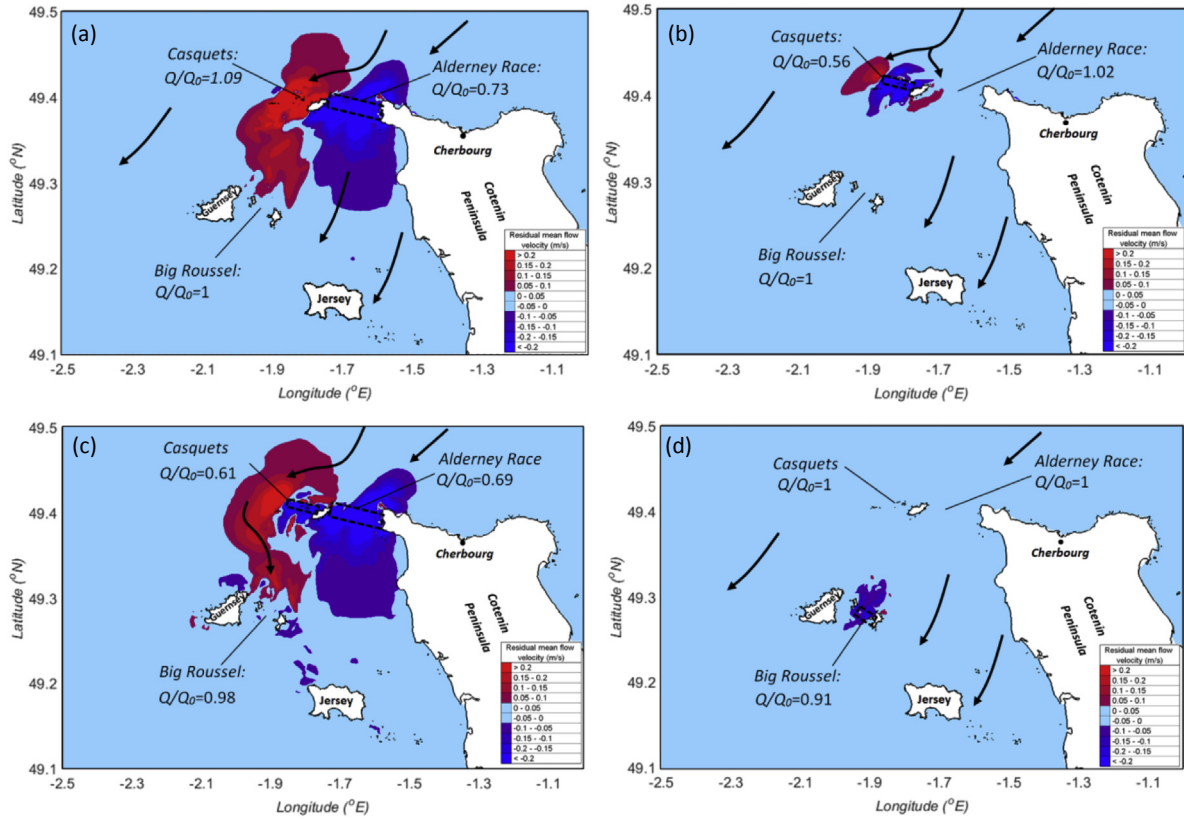
Fig. 13. Mean velocity distribution difference plots between (a) the ambient case (Scenario 1) and flow with power extraction at Alderney Race (Scenario 2) (b) the ambient case (Scenario 1) and flow with power extraction at Casquets (Scenario 3) (c) the ambient case and flow with power extraction at Alderney Race and Casquets (Scenario 5) (d) the ambient case and flow with power extraction at Big Roussel (Scenario 4). A realistic level of power extraction ($C_e = 0.015$) applied to the energy extraction zones. Arrows show the direction of the dominant ebb tide and flow diversion around Casquets. The energy extraction zones at Alderney Race and Casquets are also shown along with the change in flow rate through Big Roussel as a result of power extraction at Alderney Race and Casquets.

with the inclusion of added drag in Casquets' energy extraction zone. Power extraction at Casquets gives no change in mean flow velocities at Big Roussel.

Fig. 13c shows the change in mean velocity distribution due to power extraction at Alderney Race and Casquets together (Scenario 5) in comparison to the ambient flow. The increased drag applied uniformly over the energy extraction zones at Alderney Race and Casquets diverts flow around Casquets and into the English Channel. This enhanced flow region persists down towards Guernsey, however it does not reach Big Roussel where the mean velocity actually reduces slightly compared with the ambient case (Scenario 1), giving a 2% reduction in mean volume flux through Big Roussel and a reduction in mean extracted power of 0.01 GW (8%) compared to power extraction at Big Roussel only (Scenario 4). When power is extracted at Alderney Race *and* Casquets together,

power extraction at Casquets causes an increase in power at Alderney Race of 0.2 GW, an increase of 5%.

Fig. 13d shows that power extraction at Big Roussel (Scenario 4) has a very localised effect on mean velocities compared with the ambient case, so does not affect mean velocities in Alderney Race and Casquets, resulting in no change in mean volume flux through Alderney Race and Casquets. Power extraction at Big Roussel only (Scenario 4) gives a reduction in average volume flux through Big Roussel of 9% in comparison with the ambient case (Scenario 1).

Of all seven power extraction scenarios investigated (Table 9) using realistic C_e, the maximum extracted power still occurred with power extraction at all three sites as was the case for the upper bound simulations in §4.3 (Table 7). Using realistic C_e the mean total extracted power for the three sites working simultaneously is 4.9 GW, compared to 6.45 GW for the upper bound in Table 7. This

Table 10
Realistic average available power for Scenarios 2–8 (first presented in Table 2) using Alderney Race, Casquets and Big Roussel with an added drag coefficient, $C_e = 0.015$. Column 7 shows the realistic average extracted power from Table 9 for comparison.

Scenario	Site/Site combination	Realistic average available power (GW)				Realistic average extracted power (GW) (from Table 9)
		Alderney Race	Casquets	Big Roussel	Total for site(s)	
(1)	(2)	(3)	(4)	(5)	(6)	(7)
2	Alderney Race	1.44	–	–	1.44	3.86
3	Casquets	–	0.17	–	0.17	0.47
4	Big Roussel	–	–	0.04	0.04	0.12
5	Alderney Race & Casquets	1.51	0.29	–	1.80	4.84
6	Alderney Race & Big Roussel	1.45	–	0.04	1.49	3.99
7	Casquets & Big Roussel	–	0.18	0.04	0.22	0.69
8	Alderney Race, Casquets & Big Roussel	1.50	0.29	0.04	1.83	4.90

was made up mainly at Alderney Race (4 GW) and Casquets (0.78 GW), with Big Roussel only contributing 0.11 GW, 2% of the total extracted power.

As indicated earlier, such results have implications for site development. That is, power extraction planning within these sites will require careful, path-dependent techno-economic analysis. Authorities should consider what leasing conditions are most suitable given that sites will affect each other.

5. Conclusions

A new 2D hydrodynamic model of the English Channel was developed to simulate tidal flows around the Channel Islands at significantly improved spatial and temporal resolution than previous work. Using this model, we have carried out a systemic analysis of power extraction around the Channel Islands focussing on three sites — Alderney, Casquets and Big Roussel. The results provide estimates for the maximum average power potential at these sites which show large potential for power generation, especially at Alderney Race. We estimate that the maximum average power potential at Alderney Race is approximately 5.1 GW, which is 35% greater than that of the Pentland Firth [6], the best known site for tidal energy development in the UK. The maximum average power potential at Casquets and Big Roussel were lower but still significant at 0.47 GW and 0.24 GW respectively (Table 6).

The above results were established using upper bound limits to power extraction. However, we have demonstrated that these upper bound limits often rely on unrealistically high array packing densities, where turbines in close proximity will have a detrimental impact on device efficiency due to wake interaction. In this work we have implemented a more realistic drag coefficient C_e, resulting in reduced array density to a more realistic level. The analysis indicted that for the realistic case, the power that can be extracted is reduced by 24% (to 3.86 GW) and 50% (to 0.12 GW) at Alderney Race and Big Roussel respectively (Table 9) compared with the upper bound limits (Table 6). At Casquets there was no change in extracted power since the level of drag required to achieve the upper bound was relatively low. This is because Casquets is the least constricted site, meaning that added drag caused greater flow diversion around the site rather than a build-up in head which occurred at the more constricted sites of Alderney Race and Big Roussel. For these realistic cases the available power for electrical power generation was also calculated. At Alderney Race, Casquets and Big Roussel the average available power was 1.44 GW, 0.17 GW and 0.04 GW respectively, in total 63% lower than the extracted power from the three sites.

This work also investigated simultaneous power extraction scenarios (Table 9). Using realistic levels of drag, the maximum total extracted power occurred when power extraction was applied at all three sites as was the case for the upper bound simulations (Table 7). The mean total extracted power for the three sites working simultaneously was 4.9 GW, compared with 6.45 GW for the upper bound in Table 7. Even in the more realistic case, the Alderney Race has a higher power potential than any site in the UK.

The increase in hydraulic resistance caused by added drag in Alderney Race diverts flow around Alderney, hence increasing power extraction in Casquets by 68%. These results have implications for site development strategy, where it has been shown to be beneficial to develop Alderney Race and Casquets together as the more Alderney Race is developed, the better the resource at Casquets becomes. This is good news for simultaneous power extraction at these sites, and it would be beneficial for developers to work together to strategically position arrays in each site to maximise constructive impact on energy yield. However, currently to the authors knowledge, there is no clear regulation that takes into account such dependency. We hope that this work will provide the evidence to support the development of regulations that take into account the interdependencies between close tidal sites in the Channel Islands.

Appendix A. Telemac 2D steering file

Example steering file used to run the English Channel hydrodynamic model in Telemac 2D. Comments are added for each line to give a brief description of its purpose, which begin with a forward slash.

```
/File management///////////////////////////////////////////////////////////////////////////////////
GEOMETRY FILE                        = Geometry.slf               /Binary mesh file containing mesh coordinates
BOUNDARY CONDITIONS FILE             = Boundary_conditions.cli    /Formatted boundary conditions file
FORTRAN FILE                         = Fortran.f90                /Fortran file containing all subroutines
RESULTS FILE                         = Results.slf                /Binary results file
PARALLEL PROCESSORS                  =128                         /Number of parallel processors for
                                                                  /simulations using IRIDIS supercomputer
VARIABLES FOR GRAPHIC PRINTOUTS      = 'U,V,H,W,S'                /U,V=Flow speeds, H=Depth, W =Free surface, S= Bottom friction
GRAPHIC PRINTOUT PERIOD              = 10                         /Period between output to results file (time /steps)
LISTING PRINTOUT PERIOD              = 60                         /Period between listing file output (time /steps)
/INITIAL SETUP/////////////////////////////////////////////////////////////////////////////////////
```

(continued)

TIME STEP	= 60	|(Seconds)
NUMBER OF TIME STEPS	= 48960	|Total duration of simulation (time steps)
ORIGINAL DATE OF TIME	= 2014;11;9	|Date at initial state of simulation
		|(year;month;day)
LONGITUDE OF ORIGIN POINT	= 0.0	|Used to determine tide-generating
		|potential
LATITUDE OF ORIGIN POINT	= 36.0305	|For spherical coordinates and , which calls
		|the 'Latitu' subroutine
SPHERICAL COORDINATES	= YES	|Spherical Mercator coordinates for
		|simulations over large domains
/PHYSICAL PARAMETERS///		
CORIOLIS	= YES	|Includes the effect of the Coriolis force
TIDE GENERATING FORCE	= YES	|Includes astral forces that produce tides in
		|large domains
TURBULENCE MODEL	= 1	|Constant turbulent viscosity throughout the
		|domain
TIDAL FLATS	= YES	|Enables wetting and drying in shallow
		|regions
VERTICAL STRUCTURES	= YES	|Enables 'Dragfo' subroutine to
		|parameterise drag from tidal turbine arrays
/BOUNDARY CONDITIONS///		
LAW OF BOTTOM FRICTION	= 5	|Nikuradse friction law used to model bed
		|friction over the whole domain
FRICTION COEFFICIENT	= 0.025	|Friction coefficient relating to Nikuradse
		|friction law applied uniformly over the |domain
PRESCRIBED ELEVATIONS	= 0	|Defines elevation of open boundaries
OPTION FOR LIQUID BOUNDARIES	= 2	|Thompson method to find unknown
		| boundary velocities
/INITIAL CONDITIONS///		
INITIAL ELEVATION	= 'CONSTANT ELEVATION'	|Constant elevation across domain
INITIAL ELEVATION	= 4.0	|Magnitude of initial elevation (m)
/SOLVER SETUP///		
SOLVER	= 1	|Conjugate gradient method for the
		|hydrodynamic propagation step
SOLVER ACCURACY	= 1.E-3	|Accuracy during propagation step
DISCRETIZATIONS IN SPACE	= 12;11	|Quasi bubble triangle (4 node triangle)
		|velocity and linear depth
SUPG OPTION	= 1;1	|Upwind scheme
TYPE OF ADVECTION	= 1;5	|Type of upwind scheme: Upwind scheme
		|with classic SUPG method
TREATMENT OF THE LINEAR SYSTEM	= 2	|Uses velocity from momentum equation
		|rather than continuity equation to improve
		|computational efficiency
PRECONDITIONING	= 2	|Diagonal preconditioning (default) to speed
		|up convergence
INITIAL GUESS FOR H	= 1	|Initial value of DH equal to value of DH at
		|the previous time step (default), used to
		|speed up convergence when solving
		|propagation step
INITIAL GUESS FOR U	= 2	|Same as above but for U rather than H
FREE SURFACE GRADIENT COMPATIBILITY	= 0.9	|Relaxes continuity to remove free surface
		|wiggles
IMPLICITATION FOR DEPTH	= 0.55	|To account for semi-implicit discretization
		|of time
IMPLICITATION FOR VELOCITY &FIN	= 0.55	|To account for semi-implicit discretization
		|of time
		|End of Steering file

References

[1] Environmental Change Institute. Variability of UK marine resources. 2005. p. 12—3. Comissioned by the Carbon Trust.

[2] Black and Veatch. Phase II UK tidal stream energy resourse assessment. 2005. p. 10—31. Comissioned by the Carbon Trust.

[3] Energy Technology Support Unit. Tidal stream energy review. Harwell Laboratory; 1993. Technical report ETSU-T/05/00155/REP.

[4] European Commission. The exploitation of tidal marine currents, Wave Energy, Project results. 1996. Technical Report EUR 16683 EN.

[5] Bahaj AS, Myers L. Analytical estimates of the energy yield potential from the Alderney Race (Channel Islands) using marine current energy converters. Renew Energy Oct. 2004;29(12):1931—45.

[6] Draper S, Adcock TA, Borthwick AGL, Houlsby GT. Estimate of the tidal stream power resource of the Pentland Firth. Renew Energy Mar. 2014;63:650—7.

[7] Karsten RH, McMillan JM, Lickley MJ, Haynes RD. Assessment of tidal current energy in the Minas passage, bay of fundy. Proc Inst Mech Eng Part A J Power Energy Aug. 2008;222(5):493—507.

[8] Walters RA, Tarbotton MR, Hiles CE. Estimation of tidal power potential. Renew Energy Mar. 2013;51:255—62.

[9] Sutherland G, Foreman M, Garrett C. Tidal current energy assessment for Johnstone Strait, vancouver island. Proc IMechE Part A J Power Energy Jan. 2007;221(2):147—57.

[10] Blanchfield J, Garrett C, Rowe A, Wild P. Tidal stream power resource assessment for Masset Sound, Haida Gwaii. Proc Inst Mech Eng Part A J Power Energy Aug. 2008;222(5):485—92.

[11] Owen A. Tidal stream resource assessment for the channel islands area. 2005.

[12] Black and Veatch. UK tidal current resource and economics. 2011. p. 15—45. Commissioned by the Carbon Trust and npower, Project number 121393.

[13] Lang P, Desombre J. TELEMAC-2D software operating manual. 2013. Release 6.2.

[14] Egbert GD, Erofeeva SY, Ray RD. Assimilation of altimetry data for nonlinear shallow-water tides: Quarter-diurnal tides of the Northwest European Shelf. Cont Shelf Res 2010;30(6):668—79.

[15] Davies AM, Hall P, Howarth MJ, Knight PJ, Player RJ. Tidal currents, energy flux and bottom boundary layer thickness in the Clyde Sea and North Channel of

the Irish Sea. Ocean Dyn 2004;54(2):108–25.

[16] Lang P. TELEMAC modelling system User Manual. EDF- R&D; 2010. p. 33–4.

[17] Kapoor DC. General bathymetric chart of the oceans (GEBCO). Mar Geod 1981;5(1):73–80.

[18] Braye DI. Flow resistance in gravel-bed rivers. Gravel Bed Rivers, Fluv Process Eng Manag 1982;1:109–37.

[19] Tassi P. Sisyphe v6.3 User's manual. EDF SA; 2014. 2014.

[20] Soulsby. Dynamics of marine sands. first ed. Thomas Telford; 1997. p. 47–8.

[21] Liu Zhou. Sediment transport. first ed. Aalborg Univeristy; 1999. p. 8–10.

[22] Egbert G, Erofeeva L. OSU tidal data inversion. 2014. http://volkov.oce.orst. edu/tides/atlas.html. Date Accessed: 07/06/2014.

[23] Sustainable energy research Group. 2016 [Online]. Available, http://www. energy.soton.ac.uk/research/. Accessed: 20-May-2016.

[24] Bahaj AS, Molland AF, Chaplin JR, Batten WMJ. Power and thrust measurements of marine current turbines under various hydrodynamic flow conditions in a cavitation tunnel and a towing tank. Renew Energy Mar. 2007;32(3):407–26.

[25] Coles DS, Blunden LS, Bahaj AS. Experimental validation of the distributed drag method for simulating large marine current turbine arrays using porous fences. Int J Mar Energy Dec. 2016;16:298–316.

[26] Pawlowicz R, Beardsley B, Lentz S. Classical tidal harmonic analysis including werror estimates in MATLAB using T_TIDE. Comput Geosci 2002;28(8): 929–37.

[27] "http://noc.ac.uk/using-science/products/tidal-harmonic-analysis," [Date Accessed: 06/07/2014].

[28] UK Hydrographic Office. Admiralty tide tables United Kingdom English Channel to river humber (including isles of scilly, Channel Islands and european channel ports), 1A; 2016. NP201A.

[29] Pugh DT. Tides, surges and mean sea-level. first ed. John Wiley & Sons; 1996. p. 59.

[30] Haynes SG. The effects of array installation upon the morphology of a headland associated linear sandbank. 2015. p. 49–55. PhD: Transfer report.

[31] Pérez-Ortiz A, Pescatore J, Bryden I. A systematic approach to undertake tidal energy resource assessment with Telemac-2D. In: EWTEC 2013; 2013.

[32] European Commission. The exploitation of tidal marine currents. 1996. p. 20–5. ISBN 92-827-5658-0, Report EUR 16683 EN.

[33] Myers L, Bahaj AS. Simulated electrical power potential harnessed by marine current turbine arrays in the Alderney Race. Renew Energy Sep. 2005;30(11): 1713–31.

[34] Adcock TAA, Draper S, Houlsby GT, Borthwick AGL, Serhadlıoğlu S. The available power from tidal stream turbines in the Pentland Firth. Proc R Soc A 2013;469(2157):72–93.

[35] Garrett C, Cummins P. The power potential of tidal currents in channels. R Soc A 2005;461:2563–72.

[36] Black and Veatch. UK tidal current resource & Economics: Appendix C. 2011. p. 24–52. Commissioned by the Carbon Trust and npower, Project number 121393.

[37] Myers LE, Bahaj AS. Experimental analysis of the flow field around horizontal axis tidal turbines by use of scale mesh disk rotor simulators. Ocean Eng Feb. 2010;37(2–3):218–27.